PROCEEDINGS OF SCIENCE

Chiral extrapolation of pion scattering amplitudes and hadronic vacuum polarization

Jacobo Ruiz de Elvira,[a,*] **Gilberto Colangelo,**[b] **Martin Hoferichter,**[b] **Bastian Kubis**[c] **and Malwin Niehus**[c]

[a] *Universidad Complutense de Madrid, Departamento de Física Teórica and IPARCOS, Facultad de Ciencias Físicas, Plaza de las Ciencias 1, 28040 Madrid, Spain*

[b] *Albert Einstein Center for Fundamental Physics, Institute for Theoretical Physics, University of Bern, Sidlerstrasse 5, 3012 Bern, Switzerland*

[c] *Helmholtz–Institut für Strahlen- und Kernphysik (Theorie) and Bethe Center for Theoretical Physics, Universität Bonn, 53115 Bonn, Germany*

Chiral extrapolations are essential to connect lattice QCD simulations, often performed at unphysically large pion masses, to experimental data. In these proceedings, we summarize how the combination of dispersion relations and Chiral Perturbation Theory (ChPT) provides a controlled framework for these extrapolations in low-energy hadronic observables. We start by presenting compact analytic expressions for the one- and two-loop pion–pion partial-wave amplitudes in ChPT. We then analyze lattice-QCD data for the $\pi\pi$ P-wave scattering amplitude using the inverse amplitude method at subleading order and develop a fit strategy that allows for the first time for a stable two-loop fit. Finally, we use these results to study the pion-mass dependence of the two-pion channel in the hadronic-vacuum-polarization contribution to the anomalous magnetic moment of the muon. Our results provide valuable insight into the functional form of chiral extrapolations and even allow interpolations around the physical pion mass, providing guidance for future lattice-QCD studies.

The 11th International Workshop on Chiral Dynamics (CD2024)
26-30 August 2024
Ruhr University Bochum, Germany

*Speaker

 ISSN 1824-8039 . Published by SISSA Medialab.

PoS(CD2024)052

1. Introduction

Significant progress has been made in recent years in understanding the QCD spectrum from first principles using lattice QCD, with an increasing number of computations now performed at the physical pion mass, see, e.g., Refs. [1, 2]. However, many lattice simulations are still performed at unphysically large pion masses, see, e.g., Ref. [3], requiring a controlled chiral extrapolation to reliably connect theoretical predictions with experimental data. Furthermore, studying the QCD spectrum from lattice QCD computations requires parameterizations that enable analytic continuation into the complex plane, where resonances are characterized by their pole positions and residues. This need for analytic continuation remains essential even when lattice data is available at the physical point. Among all hadronic channels, lattice QCD has probably achieved the most remarkable success studying the $\pi\pi$ scattering P wave [1–8], rendering the ρ-channel an ideal case for investigating the detailed pion-mass dependence of hadronic observables. Furthermore, this process plays a central role in a range of phenomenological applications, including the hadronic-vacuum-polarization (HVP) contribution to the anomalous magnetic moment of the muon [9–14] and nucleon form factors [15, 16].

For perturbative observables, chiral extrapolations can be systematically performed using effective field theories, such as Chiral Perturbation Theory (ChPT). However, by construction, ChPT alone cannot be used to describe resonances, which are inherently non-perturbative phenomena. The key limitation arises from the fact that unitarity is only satisfied perturbatively in ChPT, making it insufficient for a proper resonance description. To overcome this issue, unitarization methods are required to extend the validity of chiral expansions into the resonance region. One of the most widely used techniques is the inverse amplitude method (IAM), which restores exact unitarity by analyzing the unitarity relation for the inverse amplitude [17–19]. In the elastic case, the IAM can be derived from a dispersion relation that exactly incorporates the right-hand cut discontinuity while approximating the left-hand cut using the low-energy expansion of ChPT. Thus, the IAM provides robust control over the analytic continuation into the complex plane, enabling a reliable determination of resonance pole parameters.

Writing the partial-wave for $\pi\pi$ scattering in ChPT $t(s)$ as

$$t(s) = t_2(s) + t_4(s) + t_6(s) + \cdots , \tag{1}$$

with the subscript indicating the chiral order, at next-to-leading order (NLO) the IAM formula is given by [17]

$$t^{\text{IAM}}_{\text{NLO}} = \frac{\left[t_2(s)\right]^2}{t_2(s) - t_4(s)}, \tag{2}$$

while at next-to-next-to-leading order (NNLO) it reads [18, 19]

$$t^{\text{IAM}}_{\text{NNLO}}(s) = \frac{\left[t_2(s)\right]^2}{t_2(s) - t_4(s) + \left[t_4(s)\right]^2/t_2(s) - t_6(s)}. \tag{3}$$

Thus, to apply the chiral expansion of the unitarized amplitude beyond the first term, one needs the ChPT perturbative amplitude at two-loop order. The IAM has been applied at both one- and two-loop orders to study resonance properties at unphysical pion masses [20–22] and compared with

lattice data [23, 24]. However, most analyses have been limited to one-loop order, which precludes a detailed assessment of the convergence of the expansion in the pion mass. This limitation arises from the lack of compact analytic two-loop expressions and the increased number of low-energy constants (LECs) that make the fits more volatile unless lattice data are of high quality. In order to address both points, in this work we first provide compact analytic expressions for the two-loop amplitudes and second, develop a strategy for stable two-loop fits to current lattice data, focusing on the application to the $\pi\pi$ P wave and the ρ meson. Finally, we use these results to analyze pion-mass dependence of the two-pion contribution to HVP.

2. Analytic partial-wave amplitudes in ChPT

We express the ChPT partial waves $t_{IJ}(s)$, where I and J stand for the isospin and angular momentum, respectively, in terms of the pion decay constant in the chiral limit F and the physical pion mass M_π, which makes the pion-mass dependence of the expressions more transparent. In addition, we adopt the conventions of Refs. [25–28] for the one-loop LECs l_i^r and the two-loop LECs r_i^r.

At leading order (LO), the results are [29]

$$t_{00}(s)\big|_2 = \frac{2s - M_\pi^2}{32\pi F^2}, \quad t_{20}(s)\big|_2 = -\frac{s - 2M_\pi^2}{32\pi F^2}, \quad t_{11}(s)\big|_2 = \frac{s - 4M_\pi^2}{96\pi F^2}, \quad t_{I2}(s)\big|_2 = 0, \tag{4}$$

while at NLO, the partial-wave amplitudes can be written in the form [30]

$$\mathrm{Re}\, t_{IJ}(s)\big|_4 = \sum_{i=0}^{2} b_i^{IJ}(s)\,[L(s)]^i + \sum_{i=1}^{3} b_{l_i}^{IJ}(s) l_i^r, \tag{5}$$

in terms of

$$L(s) = \log\frac{1+\sigma(s)}{1-\sigma(s)}, \qquad \sigma(s) = \sqrt{1 - \frac{4M_\pi^2}{s}}, \tag{6}$$

and coefficient functions b_i^{IJ} and $b_{l_i}^{IJ}$ given in Ref. [30], which apart from phase-space and angular-momentum factors are polynomials in s. We find that the NNLO expressions can be brought into a very similar form

$$\begin{aligned}\mathrm{Re}\, t_{IJ}(s)\big|_6 = &\sum_{i=0}^{4} c_i^{IJ}(s)\,[L(s)]^i + \sum_{i=1}^{3} c_{l_i}^{IJ}(s) l_i^r \\ &+ d^{Il}(s)\left[\sum_{n=\pm} \mathrm{Li}_3\big(\sigma_n(s)\big) - L(s)\,\mathrm{Li}_2\big(\sigma_-(s)\big)\right] + c_{l_3^2}^{IJ}(s)\big(l_3^r\big)^2 + P^{IJ}(s),\end{aligned} \tag{7}$$

where $\sigma_\pm(s) = 2\sigma(s)/(\sigma(s)\pm 1)$, the functions $c_i^{IJ}(s)$, $c_{l_i}^{IJ}(s)$, $d^{Il}(s)$ and $c_{l_3^2}^{IJ}(s)$ are given in Ref. [30] and now, in addition to powers of $L(s)$, also polylogarithms Li_n appear. The contributions from the NNLO LECs are collected in $P^{IJ}(s)$ and the imaginary parts determined by perturbative unitarity

$$\mathrm{Im}\, t_4(s) = \sigma(s)\big[t_2(s)\big]^2, \quad \mathrm{Im}\, t_6(s) = 2\sigma(s)\, t_2(s)\mathrm{Re}\, t_4(s). \tag{8}$$

In addition to the chiral extrapolation discussed in the following, these analytic expressions have also been used to calculate two-loop corrections to the Adler zero [31].

	NLO	NNLO
χ^2/dof	$216/(122-9) = 1.91$	$165/(123-15) = 1.53$
M_ρ [MeV]	761.4(5.1)(0.3)(24.7)	750(12)(1)(1)
Γ_ρ [MeV]	150.9(4.4)(0.1)(4.9)	129(12)(1)(1)
F [MeV]	88.27(0.23)(0.04)(2.86)	93.7(2.3)(0.1)(0.2)

Table 1: Results of NLO and NNLO fits to CLS data, including fit quality, ρ-resonance properties at the physical point, and the pion decay constant in the chiral limit. The first error is statistical, the second accounts for lattice spacing uncertainties, and the third represents the chiral convergence error as estimated from Eq. (11).

3. Fit to lattice data

Lattice calculations are performed in a finite volume, which means that they do not provide partial waves t_{IJ} or their corresponding phase shifts δ_{IJ}, but instead yield discrete energy values E_{IJ}^{lat}. In the elastic region, these energy levels E are related to the phase shift via a quantization condition of the form,

$$\cot\left[\delta\left(E\right)\right] = \mathcal{Z}\left(E\right), \tag{9}$$

where $\mathcal{Z}$ is a known analytic function that depends on the lattice setup. Thus, to fit lattice data, we first compute the phase shift δ_{IJ} using the IAM at either NLO or NNLO for fixed values of the LECs. Next, we insert δ_{IJ} into Eq. (9) to determine the corresponding IAM-predicted energy levels E_{IJ}^{IAM}. The LECs are then varied to minimize the function

$$\chi^2 \equiv \sum_{k,j} \left(E_k^{\text{lat}} - E_k^{\text{IAM}}\right) C_{kj}^{-1} \left(E_j^{\text{lat}} - E_j^{\text{IAM}}\right), \tag{10}$$

where the sum runs over the different energy levels obtained on the lattice and C is their corresponding correlation matrix.

To illustrate our fitting strategy and explore the pion-mass dependence, we focus on the $\pi\pi$ scattering P wave—the δ_{11} phase shift and the ρ-meson parameters—and analyze the data from Ref. [4], which is based on gauge configurations generated by the CLS collaboration and includes six ensembles at five different pion masses in the range 200 MeV to 284 MeV. In addition, given the strong connection between the ρ-meson properties and the pion decay constant [32], we also incorporate the F_π determination from Ref. [33] into our fit.

At LO the only free parameters are the pion decay constant in the chiral limit F and the pion mass M_π. At NLO, additional LECs appear, namely the combination $l_2^r - 2l_1^r$ and l_4^r. At NNLO the expressions further depend on l_{1-4}^r as well as $r_{a,b,c,F}$ [30]. Moreover, a reliable uncertainty estimate must account for three key sources of error: first, the statistical errors from the lattice data; second, the lattice spacing uncertainty, which affects the ChPT expressions via the renormalization scale μ [30]. To mitigate its effect, we work in lattice units wherever possible. Third, the truncation errors in the chiral expansion in Eq. (1), which we assess by comparing IAM results at one- and two-loop order. The chiral expansion proceeds in s/M_ρ^2 as well as $\alpha = M_\pi^2/M_\rho^2$, with M_ρ serving as the expected breakdown scale—the lowest-lying resonance in this partial wave. Since the IAM

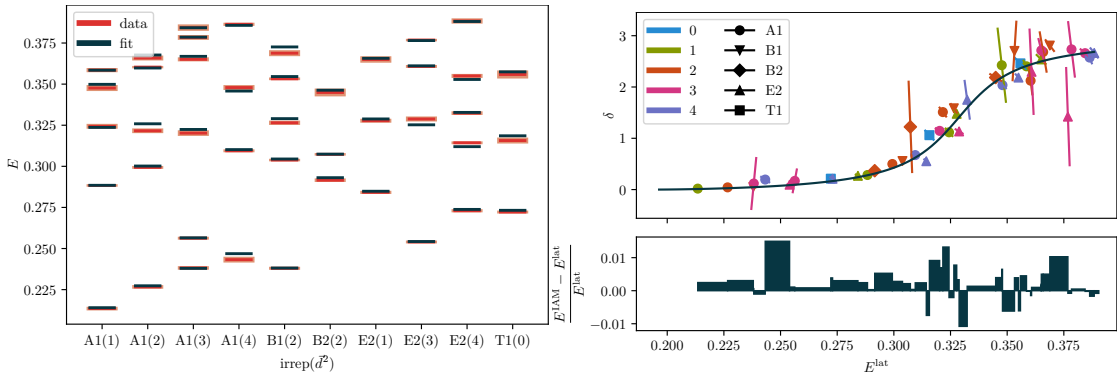

Figure 1: Results from a global NNLO fit to the CLS data, compared with ensemble D101. Left: Energy levels: Each column represents a different combination of boost momentum and irrep [30]. Right: Corresponding scattering phase: The color indicates the boost momentum, while the symbol shape denotes the irrep. The solid curve shows the fit result, and the bottom panel plots the relative differences between the IAM-predicted and lattice energy levels. Figures taken from Ref. [30].

resums the energy dependence through unitarization, the pion-mass expansion remains the most critical factor. Following Ref. [34], we estimate the truncation error of an observable X as

$$\begin{aligned} \Delta X_{\mathrm{NLO}} &= \alpha X_{\mathrm{NLO}}, \\ \Delta X_{\mathrm{NNLO}} &= \max\left\{\alpha^2 X_{\mathrm{NLO}}, \alpha\left|X_{\mathrm{NLO}} - X_{\mathrm{NNLO}}\right|\right\}. \end{aligned} \tag{11}$$

The fit results are summarized in Table 1. In general, the χ^2/dof improves significantly when going from NLO to NNLO, although achieving a fully acceptable fit will require a deeper understanding of lattice artifacts. For illustration, Fig. 1 shows the energy levels and phase shift obtained from the NNLO fit to the CLS data for a single ensemble.

Since the IAM amplitude has the appropriate analytic structure, it can be analytically continued to the second Riemann sheet, where the pole associated with the ρ resonance is located. Extracting the mass M_ρ and width Γ_ρ from the pole position s_{p} via $s_{\mathrm{p}} = (M_\rho - i\Gamma_\rho/2)^2$ yields the values shown in Table 1. A comparison with the ρ parameters derived from Roy-like equations [35, 36] reveals that both the NLO and NNLO results are statistically compatible, with a 1.4σ discrepancy in the width at NNLO. However, only the NLO value of F is compatible with the literature value $F = 86.89(58)$ MeV, which is obtained by combining the PDG value of F_π [37] with the FLAG $N_{\mathrm{f}} = 2 + 1$ average of F_π/F [38].

Our main results are summarized in Fig. 2, where we show the extrapolated phase at the physical pion mass from fits to the CLS data, and the pion-mass dependence of the decay constant and the ρ parameters. Notably, the two-loop analysis significantly improves precision beyond the physical point, where truncation errors become dominant. Moreover, the overlapping error bands at NLO and NNLO—assuming a breakdown scale set by M_ρ—suggest that the true breakdown scale of the theory is slightly below the ρ mass, but not by a large margin.

A similar strategy to extrapolate lattice-QCD data, relying on the IAM $\pi\pi$ phase shifts at variable pion mass, has been used in Ref. [39] to extrapolate lattice data for $\gamma\pi \to \pi\pi$ [40, 41] to the physical point and thereby extract the chiral anomaly [42, 43].

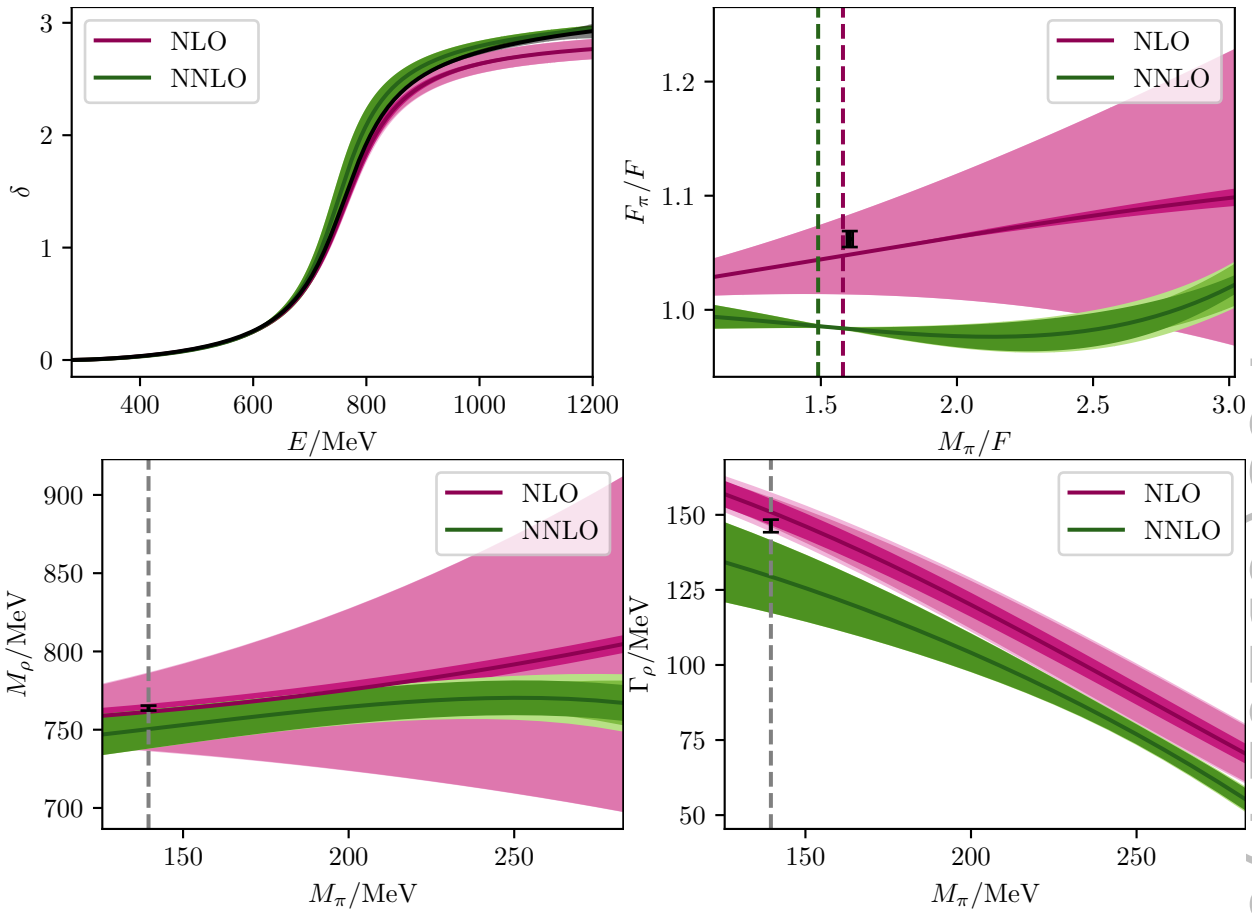

Figure 2: Top left: Extrapolated phase at the physical pion mass from global fits to the CLS data; the black curve shows the result from the dispersive analysis in Ref. [9] for comparison. Top right: Pion-mass dependence of the decay constant, expressed in units of F to minimize scale-setting effects. The black band indicates the reference value from Ref. [38]. Bottom: The ρ meson mass and width as determined from the CLS data fits; the black bands denote the reference values from Ref. [35]. In all panels, the error bands (from darkest to lightest) correspond to the data error (statistical plus spacing), the truncation error, and the total error, respectively. Dashed lines mark the physical pion mass. Figures taken from Ref. [30].

4. Pion-mass dependence of the two-pion contribution to HVP

To resolve the tensions both within data-driven determinations of HVP [9–14, 44–56] and with lattice QCD [57–60], it is important to scrutinize all aspects of the evaluation, one of which concerns the pion-mass dependence of the leading two-pion channel. The two-pion contribution to the HVP crucially depends on the pion vector form factor $F_\pi^V(s)$, which can be factorized as

$$F_\pi^V(s) = \Omega_1^1(s) \times G_\omega(s) \times G_{\text{in}}(s). \tag{12}$$

Here, the three terms incorporate two-pion, three-pion, and higher intermediate states, respectively. The Omnès factor $\Omega_1^1(s)$ [61] accounts for the effect of the P-wave $\pi\pi$ scattering phase shift, $G_\omega(s)$ describes ρ–ω mixing through the residue ϵ_ω at the ω pole, and $G_{\text{in}}(s)$ is expanded in a

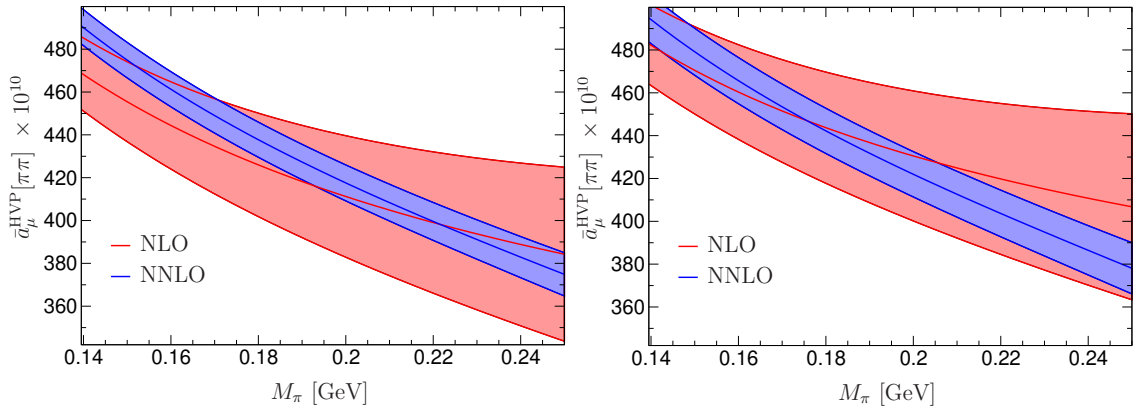

Figure 3: Pion-mass dependence of $\bar{a}_\mu^{\rm HVP}[\pi\pi]$ from the NLO (red) and NNLO (blue) IAM, for a normal (left) and conformal (right) polynomial. Figures taken from Ref. [65].

(conformal) polynomial, with parameters matched to the pion charge radius $\langle r_\pi^2 \rangle$ and higher orders in the low-energy expansion of $F_\pi^V(s)$.

Here, we focus on the pion-mass dependence of the pure $I = 1$ correlator by setting $\epsilon_\omega = 0$ in Eq. (12) and employing the pion-mass dependence of δ_{11} at NLO and NNLO order [30] as described in the previous section. The relevant parameters are now determined from a combined fit to lattice QCD data [4] and phenomenological results [9]. For $G_{\rm in}(s)$, we use the known two-loop expansion of $\langle r_\pi^2 \rangle$ [62]. Here, the main uncertainty arises from a new low-energy constant $r_{V1}^r = 2.0 \times 10^{-5}$, which we estimate from resonance saturation and validate with lattice-QCD calculations of $\langle r_\pi^2 \rangle$ at larger-than-physical pion masses [63, 64].

The resulting prediction for the pion-mass dependence, shown in Fig. 3, successfully reproduces the value at the physical point within uncertainties. Potential applications to lattice QCD are explored in Ref. [65], including a comprehensive fit of the $I = 1$ contribution and tests of the strength of infrared singularities in the relevant fit region [66].

Finally, to investigate potential isospin-breaking effects, we evaluate the difference between the two-pion contribution to the HVP from the charged and neutral pion masses:

$$a_\mu^{\rm HVP}[\pi\pi]\big|_{M_{\pi^\pm}} - a_\mu^{\rm HVP}[\pi\pi]\big|_{M_{\pi^0}} = -7.67(4)_{\rm ChPT}(3)_{\rm polynomial}(4)_{\langle r_\pi^2 \rangle}(21)_{r_{V1}^r}[22]_{\rm total}, \tag{13}$$

where the uncertainties are attributed to chiral convergence, differences between a standard and conformal polynomial, and the uncertainties in $\langle r_\pi^2 \rangle$ and r_{V1}^r, respectively. This effect is primarily driven by the threshold region, leading to a contribution that is almost entirely contained within the long-distance window, see Ref. [12].

5. Conclusions

In this contribution, we first presented compact analytic expressions for the one- and two-loop partial-wave amplitudes for $\pi\pi$ scattering. These expressions have subsequently been used to analyze lattice data for the P-wave amplitude and extract the ρ-meson parameters using the IAM. Our results show that two-loop fits significantly improve the fit quality, and the comparison between NLO and NNLO results indicates that the breakdown scale of the chiral expansion is close

to the expected scale set by the ρ mass. Our analysis also reveals that the current lattice data sets cannot be described in a statistically satisfactory manner, highlighting the need for a more detailed understanding of lattice systematics.

Finally, we showed how these results can be used to control the quark-mass dependence of the HVP contribution to the anomalous magnetic moment of the muon by focusing on the $I = 1$ two-pion channel. While a direct application of ChPT is not possible due to its limited range of convergence [66], we have demonstrated that this challenge can be overcome using the IAM, which reproduces the expected HVP value and constrains the chiral extrapolation of HVP calculations in lattice QCD performed at larger-than-physical quark masses. Furthermore, our one- and two-loop implementations allowed us to study the behavior of the chiral convergence and assess the corresponding systematic uncertainties.

Acknowledgments

Financial support by the SNSF (Project Nos. TMCG-2_213690 and 200020_200553), the Ramon y Cajal program (RYC2019-027605-I) of the Spanish MICIU and the Spanish Ministerio de Ciencia e Innovacion (Project PID2022-136510NB-C31) are gratefully acknowledged.

References

[1] P. Boyle *et al.*, Phys. Rev. D **111**, 054510 (2025).

[2] P. Boyle *et al.*, Phys. Rev. Lett. **134**, 111901 (2025).

[3] A. Rodas *et al.* (Hadron Spectrum), Phys. Rev. D **108**, 034513 (2023).

[4] C. Andersen, J. Bulava, B. Hörz, and C. Morningstar, Nucl. Phys. B **939**, 145 (2019).

[5] M. Werner *et al.* (ETM), Eur. Phys. J. A **56**, 61 (2020).

[6] F. Erben, J. R. Green, D. Mohler, and H. Wittig, Phys. Rev. D **101**, 054504 (2020).

[7] M. Werner *et al.* (ETM), Eur. Phys. J. A **56**, 61 (2020).

[8] M. Fischer *et al.* (ETM), Phys. Lett. B **819**, 136449 (2021).

[9] G. Colangelo, M. Hoferichter, and P. Stoffer, JHEP **02**, 006 (2019).

[10] G. Colangelo, M. Hoferichter, and P. Stoffer, Phys. Lett. B **814**, 136073 (2021).

[11] G. Colangelo, M. Hoferichter, B. Kubis, and P. Stoffer, JHEP **10**, 032 (2022).

[12] M. Hoferichter *et al.*, Phys. Rev. Lett. **131**, 161905 (2023).

[13] P. Stoffer, G. Colangelo, and M. Hoferichter, JINST **18**, C10021 (2023).

[14] T. P. Leplumey and P. Stoffer, (2025), arXiv:2501.09643 [hep-ph].

[15] M. Hoferichter *et al.*, Eur. Phys. J. A **52**, 331 (2016).

[16] M. Hoferichter, B. Kubis, J. Ruiz de Elvira, and P. Stoffer, Phys. Rev. Lett. **122**, 122001 (2019), [Erratum: Phys. Rev. Lett. **124**, 199901 (2020)].

[17] A. Dobado, M. J. Herrero, and T. N. Truong, Phys. Lett. B **235**, 134 (1990).

[18] A. Dobado and J. R. Peláez, Phys. Rev. D **56**, 3057 (1997).

[19] J. Nieves, M. Pavon Valderrama, and E. Ruiz Arriola, Phys. Rev. D **65**, 036002 (2002).

[20] C. Hanhart, J. R. Peláez, and G. Ríos, Phys. Rev. Lett. **100**, 152001 (2008).

[21] J. R. Peláez and G. Ríos, Phys. Rev. D **82**, 114002 (2010).

[22] J. Nebreda and J. R. Peláez, Phys. Rev. **D81**, 054035 (2010).

[23] B. Hu, R. Molina, M. Döring, M. Mai, and A. Alexandru, Phys. Rev. D **96**, 034520 (2017).

[24] R. Molina and J. Ruiz de Elvira, JHEP **11**, 017 (2020).

[25] J. Gasser and H. Leutwyler, Annals Phys. **158**, 142 (1984).

[26] J. Bijnens, G. Colangelo, G. Ecker, J. Gasser, and M. E. Sainio, Phys. Lett. B **374**, 210 (1996).

[27] J. Bijnens, G. Colangelo, G. Ecker, J. Gasser, and M. E. Sainio, Nucl. Phys. B **508**, 263 (1997), [Erratum: Nucl.Phys.B 517, 639–639 (1998)].

[28] J. Bijnens, G. Colangelo, and G. Ecker, Annals Phys. **280**, 100 (2000).

[29] S. Weinberg, Phys. Rev. Lett. **17**, 616 (1966).

[30] M. Niehus, M. Hoferichter, B. Kubis, and J. Ruiz de Elvira, Phys. Rev. Lett. **126**, 102002 (2021).

[31] L. A. Heuser *et al.*, Eur. Phys. J. C **84**, 599 (2024).

[32] J. Ruiz de Elvira, U.-G. Meißner, A. Rusetsky, and G. Schierholz, Eur. Phys. J. C **77**, 659 (2017).

[33] M. Bruno, T. Korzec, and S. Schaefer, Phys. Rev. D **95**, 074504 (2017).

[34] E. Epelbaum, H. Krebs, and U.-G. Meißner, Eur. Phys. J. A **51**, 53 (2015).

[35] García-Martin *et al.*, Phys. Rev. Lett. **107**, 072001 (2011).

[36] M. Hoferichter, J. Ruiz de Elvira, B. Kubis, and U.-G. Meißner, Phys. Lett. B **853**, 138698 (2024).

[37] P. A. Zyla *et al.* (Particle Data Group), PTEP **2020**, 083C01 (2020).

[38] S. Aoki *et al.* (FLAG), Eur. Phys. J. C **80**, 113 (2020).

[39] M. Niehus, M. Hoferichter, and B. Kubis, JHEP **12**, 038 (2021).

[40] R. A. Briceño *et al.*, Phys. Rev. D **93**, 114508 (2016), [Erratum: Phys. Rev. D **105**, 079902 (2022)].

[41] C. Alexandrou *et al.*, Phys. Rev. D **98**, 074502 (2018), [Erratum: Phys. Rev. D **105**, 019902 (2022)].

[42] M. Hoferichter, B. Kubis, and D. Sakkas, Phys. Rev. D **86**, 116009 (2012).

[43] M. Hoferichter, B. Kubis, and M. Zanke, Phys. Rev. D **96**, 114016 (2017).

[44] T. Aoyama *et al.*, Phys. Rept. **887**, 1 (2020).

[45] M. Davier, A. Hoecker, B. Malaescu, and Z. Zhang, Eur. Phys. J. C **77**, 827 (2017).

[46] A. Keshavarzi, D. Nomura, and T. Teubner, Phys. Rev. D **97**, 114025 (2018).

[47] M. Hoferichter, B.-L. Hoid, and B. Kubis, JHEP **08**, 137 (2019).

[48] M. Davier, A. Hoecker, B. Malaescu, and Z. Zhang, Eur. Phys. J. **C80**, 241 (2020), [Erratum: Eur. Phys. J. **C80**, 410 (2020)].

[49] A. Keshavarzi, D. Nomura, and T. Teubner, Phys. Rev. **D101**, 014029 (2020).

[50] B.-L. Hoid, M. Hoferichter, and B. Kubis, Eur. Phys. J. C **80**, 988 (2020).

[51] A. Crivellin *et al.*, Phys. Rev. Lett. **125**, 091801 (2020).

[52] A. Keshavarzi, W. J. Marciano, M. Passera, and A. Sirlin, Phys. Rev. D **102**, 033002 (2020).

[53] B. Malaescu and M. Schott, Eur. Phys. J. C **81**, 46 (2021).

[54] D. Stamen *et al.*, Eur. Phys. J. C **82**, 432 (2022).

[55] G. Colangelo *et al.*, Phys. Lett. B **833**, 137313 (2022).

[56] M. Hoferichter, B.-L. Hoid, B. Kubis, and D. Schuh, JHEP **08**, 208 (2023).

[57] A. Boccaletti *et al.* (BMWc), (2024), arXiv:2407.10913 [hep-lat].

[58] T. Blum *et al.* (RBC, UKQCD), (2024), arXiv:2410.20590 [hep-lat].

[59] D. Djukanovic *et al.*, (2024), arXiv:2411.07969 [hep-lat].

[60] A. Bazavov *et al.* (Fermilab Lattice, HPQCD, MILC), (2024), arXiv:2412.18491 [hep-lat].

[61] R. Omnès, Nuovo Cim. **8**, 316 (1958).

[62] J. Bijnens, G. Colangelo, and P. Talavera, JHEP **05**, 014 (1998).

[63] X. Feng, Y. Fu, and L.-C. Jin, Phys. Rev. D **101**, 051502 (2020).

[64] G. Wang *et al.* (χQCD), Phys. Rev. D **104**, 074502 (2021).

[65] G. Colangelo *et al.*, Phys. Lett. B **825**, 136852 (2022).

[66] M. Golterman, K. Maltman, and S. Peris, Phys. Rev. D **95**, 074509 (2017).